

Time-Domain Microwave Breast Cancer Detection: Extensive System Testing with Phantoms

www.tcrt.org
DOI: 10.7785/tcrt.2012.500307

Emily Porter, M.Eng.^{1*}
Adam Santorelli, M.Eng.¹
Mark Coates, Ph.D.¹
Milica Popović, Ph.D.¹

Early detection of breast cancer is known to be a key factor in the successful treatment of the disease. Here, we present a detection technique complementary to the currently used modalities (primarily mammography, ultrasound and magnetic resonance imaging). Our time-domain breast cancer detection system transmits microwave-range pulses into the breast and records the scattering off of the breast in order to detect malignancies. This method is made possible by an intrinsic contrast in the dielectric parameters, specifically the relative permittivity and conductivity, of the healthy and malignant breast tissues over the microwave frequency range. The long-term goal of our work is to develop a system that can be used periodically to monitor for unusual changes in breast tissues; for instance, healthy breasts would be scanned, and follow-up scans at regular intervals would detect any small changes in breast tissue composition that could indicate the presence of a malignant growth. At that point, the patient would be referred to see a doctor for further investigation of the abnormal results. Such a system would compare each new scan with previous ones to determine the level of tissue changes, and would be used by patients at home. We report feasibility and performance tests for our initial system, conducted with breast phantoms made up of tissue-mimicking materials (unique skin, fat, gland and tumor mixtures). We initiated the system testing with simple homogeneous phantoms, consisting solely of adipose tissue. Then, we extended our tests to cases of increasing complexity by adding a skin layer and varying percentages of glandular structures and tumor sizes. In order to optimize the experimental system, we performed tests with multiple antenna arrangements, tumor sizes and locations. This work shows that there are specific antenna arrangements that are advantageous for tumor detection and demonstrates the capabilities of our time-domain microwave breast tumor detection system.

¹Department of Electrical and Computer Engineering, McConnell Building, McGill University, 3480 University Montreal, Canada, H3A 0E9

Key words: Cancer detection; Microwave imaging; Microwave propagation; Phantoms.

Introduction

Microwave imaging for breast cancer detection is an area of research that is rapidly expanding. Based on the inherent contrast in the dielectric properties of healthy and malignant breast tissues over the microwave frequency range (1), microwave techniques have the potential to detect cancerous growths within the breast. The current standard method for breast cancer detection is x-ray mammography. Mammograms are widely available to patients for screening, and in the time since their adoption in hospitals and clinics breast cancer fatality rates have decreased (2). Unfortunately, this technique has many downsides: mammograms

*Corresponding author:
Emily Porter, M.Eng.
Phone: 1 (514) 817-4503
E-mail: emily.porter@mail.mcgill.ca

Abbreviations: FWHM: Full-Width at Half-Maximum; 3-D: 3-Dimensional; DC: Direct Current; TWTLTA: Traveling Wave Tapered and Loaded Transmission Line Antenna; UWB: Ultrawideband.

use breast compression (which can be painful to the patient), as well as ionizing radiation (which may be harmful in frequently repeated doses (3)). Also, mammography has been plagued by undesirably high false-negative and false-positive rates (4), in other words, frequently missing incidences of cancer, or unnecessarily requiring patients to undergo further testing. These drawbacks motivate the search for alternative or complementary breast cancer detection technologies.

Microwave systems aim to provide non-invasive, pain-free, cost-efficient detection with no ionizing radiation. Several microwave breast cancer detection systems have already been proposed. The literature focuses on techniques that utilize frequency-domain measurements. Researchers at the University of Bristol have implemented a 60-element array that performs 1770 multi-static measurements in only 10 seconds using a vector network analyzer (5). Their system operates over the 4 to 8 GHz range, and is currently undergoing clinical trials. Another advanced system design developed at Dartmouth College (6), (7) has also undergone clinical trials. This system uses 16 monopole antennas operated in the 0.5-3 GHz frequency range. One antenna transmits at a fixed frequency, while the other 15 receive, then the transmitting antenna is switched, allowing for 240 measurements in every plane of the array (6). The array can be moved to various planes in order to reconstruct a 3-D image.

The system we present here, on the other hand, is based on time-domain measurements. We attempt only to detect the tumor and not to reconstruct a complete dielectric profile of the breast. In fact, the aim of our work is to develop an early, at home detection system that would allow a patient to undergo scans at regular intervals and would compare the past healthy breast scans to the current scan to determine if there exist any tissue abnormalities. A similar method of differential assessment has been applied with promising results by Byrne *et al.* in (8) on numerically-generated data sets. In our work, detection would also be performed using a comparison of the data sets, with the output being either a positive or negative signal (abnormality present or not); no images would be created with this methodology. Our system transmits time-domain pulses of 70 ps duration, covering a span of frequencies from DC to 14 GHz. Such a design allows us to record both low frequency (low attenuation) and high frequency (high resolution) information at the same time; and allows the scan duration to be very brief. It also requires less computational complexity than do methods involving frequency-domain measurements with time-domain algorithms.

The goal of the work presented here is to identify whether or not the given system is able to detect a difference in signals from a breast with a tumor present and the same breast with no tumor. The results will guide us in our steps to modify the system in the immediate near future. Our system currently

allows for 16 antennas, leading to 240 possible signals recorded in multistatic radar arrangement. As the current goal of our prototype is to indicate whether a tumor is present (and not necessarily to locate or image it) by comparing breast scans to past healthy scans performed on the same patient, we may not require more than 240 recordings. This 16-antenna arrangement has allowed us to detect tumors in simple phantoms; however, the number of required signals remains to be determined for detecting tumors in patients. We do note that should more signals be necessary, the system in its present form can be easily adapted to fit an array of 32 or even 48 antennas. The test results presented here will allow us to arrange the antennas within an updated array in the most favorable manner from the standpoint of detection.

Materials and Methods

Time-Domain Measurement System

Our initial breast cancer detection system was introduced in (9). We describe the system in further detail here, and highlight recent improvements that we have made. The main elements of our system are the following: an impulse generator, a clock, an oscilloscope, broadband antennas and a radome. The impulse generator (Picosecond Pulse Labs, (10), Impulse Generator Model 3600) sends a pulse of approximately -7.5 V, with 70 ps full-width at half-maximum (FWHM), to the transmitting antenna on every clock (Tektronix (11), gigaBERT 1400 generator) signal. The clock runs at 25 MHz (250 MHz in earlier tests, as will be noted in later sections). The transmitting antenna is placed in a slot in a hemi-spherical bowl-shaped radome, which holds within it the breast phantom under test. The wave propagates into the breast phantom from the transmitting antenna, where it is attenuated and scatters at each tissue interface. The receiving antenna, placed in a different slot in the radome, then picks up the scattered wave. All tests use only two antennas; however, the current design allows for a 16-element multistatic array and is easily adaptable up to 32 elements. The receiving antenna feeds into an oscilloscope (Pico Technology (12), PC Oscilloscope 9201), which is USB connected to a computer, allowing for storage and processing of the received data. The measurement process and equipment is shown in the system schematic in Figure 1.

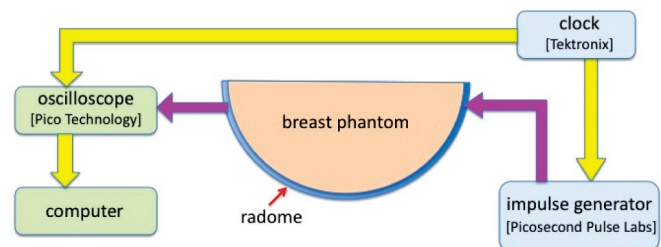


Figure 1: Schematic of time-domain measurement system.

The antenna we use in our system is the Traveling Wave Tapered and Loaded Transmission Line Antenna (TWTLTLA), designed specifically for biological sensing (13). In particular, it is built on a substrate with dielectric constant $\epsilon_r = 10.2$, and is fashioned so as to have optimal performance when operating in a medium with similar relative permittivity. This compact, planar antenna measures only $0.635 \times 12 \times 15.8 \text{ mm}^3$. The wideband performance is obtained by using constant resistive loading (surface resistivity of $50 \Omega/\text{square}$, or equivalently, a conductivity σ of 1142.8 S/m). This end-fire antenna is easily fabricated and relatively sturdy, with fidelity above 0.95 and efficiency of 39% (13). The model of the TWTLTLA is shown in Figure 2, along with a photograph of the final fabricated antenna.

We designed a radome to hold the antennas securely in place while measurements are underway. The radome is made of Alumina (Al_2O_3), $\epsilon_r \approx 9.6$, and was fabricated from our design by Friatec (14). We chose this material based on its advantageous properties: low-loss, dielectric constant similar to that of the antenna substrate (for good matching), and low moisture absorption. Alumina is also strong enough not to fracture or break during the antenna slot drilling process. The radome, with dimensions and photograph shown in Figure 3, is a hemi-spherical bowl with an outer radius of 8.5 cm and an inner radius of 7 cm. This allows for a breast phantom with a maximum diameter of 14 cm. Sixteen antennas can be held in the radome; there are four slots along the exterior surface of each quadrant. A diagram of the radome with the slots uniquely numbered is depicted in Figure 3; allowing for an easy description of where the antennas are placed in each measurement scenario. Some slots are oriented similarly, while some are at 90° , allowing the antennas to be placed in such a manner as to receive either the co-polarized or cross-polarized response. The slots are slightly larger than the dimensions of the antenna – this was a design choice, to ease the manufacturing challenge of drilling slots as thin as 0.635 mm. To avoid air gaps between the antenna and the slot

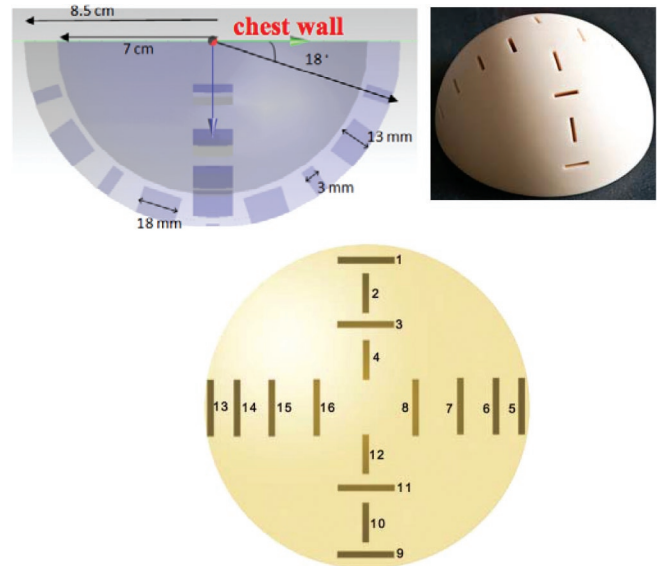


Figure 3: Drawing with dimensions shown (top left) and photograph (top right) of the radome. Also shown is a top view of the radome with all antenna slots numbered (bottom).

walls we use ‘suitcases’, enclosures that look like a container with a lid and a smaller slot that tightly fits the antenna. Thus we place the antennas in the suitcases, and then slide the suitcases into the slots in the radome. The suitcases are made of low-loss dielectric Eccostock HiK (fabricated by Emerson & Cuming (15)), with $\epsilon_r = 10$. The suitcase design details and dimensions can be found in (16).

We measure the return loss (S_{11}) of the antenna, in a suitcase in the radome. For this measurement, the radome is filled with a breast phantom made of a thin skin layer and homogeneous fat-mimicking tissue; and, in between the phantom’s skin and the radome is a matching medium. The resulting S_{11} is plotted in Figure 4. We perform the return loss measurement at two antenna positions within the radome to ensure consistency in the phantom properties. From the plot, we see that the S_{11} for both positions is similar, which shows that, as expected, the phantom’s dielectric properties do not vary significantly from one point to another. The antenna in this system performs best above 3 GHz, with a return loss near or below -10 dB .

Description of Breast Phantoms

The tissue phantoms have been thoroughly described in our past work (17). We make four tissue-mimicking phantoms: fat, skin, tumor and gland, out of commonly available chemicals. The tissue phantoms are each designed to have relative permittivity and conductivity similar to those of the actual tissues, as reported in measurements in the literature (1). The tissue phantom’s fabrication procedure is presented in (17) and their updated electrical property measurements are

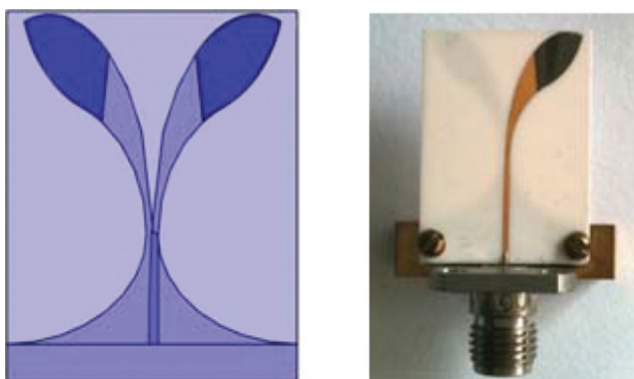


Figure 2: Drawing (left) and photograph (right) of the TWTLTLA. The antenna measures $0.635 \times 12 \times 15.8 \text{ mm}^3$.

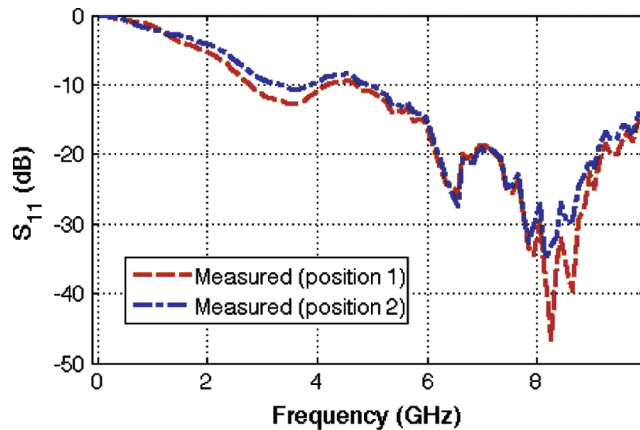


Figure 4: Measured S_{11} for antennas in two positions within the radome.

given in (18). In (19), advanced heterogeneous breast phantoms have also been reported. While our phantoms are made with different materials and physical dimensions, the key improvement, in contrast to the phantoms created in (19), is in the electrical parameters of our glandular structures. The heterogeneities in (19) are composed of materials with relative permittivity $\epsilon_r = 10$ -30, with a tumor ϵ_r of 50, leading to a malignant/healthy contrast of between 5:1 and 1.6:1. In our phantoms, there is an approximately 5.5:1 contrast in the dielectric constant of tumor to fat tissues, while the contrast between the malignant and glandular tissue is much less, on the order of 10% (18). In fact, our gland phantom has a ϵ_r of about 50 at 2 GHz, a value much closer to that of actual glandular tissue reported in the literature (1).

Using the individual tissue phantoms, we build comprehensive breast phantoms that include up to all four tissue types. A typical breast phantom is hemi-spherical with a 6.5-cm radius. It includes a 2.5-mm thick layer of skin, filled with a mixture of fat and glandular tissue, with a single tumor located somewhere within the phantom. For all phantom tests, we fill the space in between the phantom's surface and the radome in which it is placed with a matching medium (approximately 0.5 cm thick) made of the fat-mimicking material. This matching medium serves mainly to eliminate the possibility of any air gaps existing between the breast and the radome, as air gaps can negatively and unpredictably affect the signals received at the antenna.

Since the breast phantoms used in each set of experiments differ in tissue composition and organization, the specifics of each test phantom will be described later. A complete description of the corresponding system test will also be provided. We performed all phantom tests within a week of the phantom fabrication, to ensure that no dehydration had occurred and thereby avoiding any change in the tissues' dielectric properties.

Measurement Procedure

For each system test, we start by placing the test phantom into the radome. Then we arrange the antennas, which are already connected to the rest of the system, in the desired radome slots. A baseline measurement is taken first: a recording of the 'healthy response', the received signal when no tumor-mimicking tissues (here forth referred to just as 'tumor(s)') are present in the test phantom. After we obtain the baseline signal, we insert the tumor under test into the chosen site within the breast phantom. Once the tumor is in the breast phantom, the signal at the receiving antenna is re-recorded. In our work, we calculate and define the tumor response as the difference between the received signal when the tumor is in the breast, and the healthy baseline. We have previously performed tests using 'dummy' tumors that allowed us to confirm the tumor response is in fact a result of the malignant tissue being added to the breast and not due to the insertion process of the tumor into the breast phantom.

We note that the baseline measurement is not feasible in a clinical setting and we do not intend for it to be used as such. It is an intermediate step that allows us to obtain data about the presence of tumors within the breast phantoms very easily, without excessive signal processing. Conducting experiments that rely on generating an image by applying a signal processing technique conflates the performance of the imaging methodology (which includes calibration) and the performance of the measurement apparatus. Our goal in this paper is to assess solely the performance of the measurement apparatus to determine whether it generates a detectable signal and which configurations perform best. If the signal is not detectable when a baseline is present, there is no hope of detection when additional challenges arise. Experiments presented here on the measurement system allow us to learn from the tumor responses in various scenarios, and adapt the system into an optimized form.

We use the peak received amplitude and peak tumor response as two key metrics with which to analyze our system's performance. For successful detection, it is important that they both be above the noise level, and that the tumor response is clearly seen in the time-domain signals. The peak received value is determined as the maximum of the absolute value of the recorded signal. Similarly, the peak tumor response is calculated as the maximum of the absolute value of the tumor response.

Test 1 Description: Fat-Only Breast Phantoms

As an initial experiment, we test our system's tumor detection abilities with the simplest type of breast phantom: a phantom made entirely of fat (no skin or heterogeneities). For this series of tests, the clock frequency is always set to 250 MHz. We use two sizes of tumor for this series of experiments. Both tumors are relatively large, since the primary goal of this

series of tests is to identify promising antenna and system configurations rather than explore the detection limits of the system. The tumors are cylindrical in shape with 3-cm height and diameters of 1 cm and 2 cm, respectively. We carve the tumor phantoms manually, so they have a rough, uneven surface.

Test 1 is comprised of 7 cases, each with a different antenna arrangement. Within each antenna arrangement, both tumor sizes are positioned at each of two or three places within the phantom. Thus, there are up to seven recordings per case, including the baseline. For example, Case 1 has three tumor sites (one near the transmitter, one in the center of the radome, and one near the receiver) and there are two tumor sizes, so with the baseline there are seven recordings for this case. This leads to a total of 39 measurements, a comprehensive list of which is shown in Table I. This testing of scenarios is thorough; we test every possible type of antenna layout – transmission and reflection scenarios, and each of those with both cross- and co-polarized antenna orientations.

In Table I, we present the list of cases (determined by the antenna arrangements), along with a schematic drawing of each case scenario. The antennas are located in the second or third slot away from the chest wall, as the geometry allows. As such, in Cases 1 and 4 both the transmitting and receiving antennas are in the second slot from the chest (slot numbers 6 and 14 for Case 1, as per Figure 3; slot numbers 6 and 10 for Case 4), Cases 2, 5 and 7 have the transmitter in the second slot and receiver in the third (slot numbers 2 and 11 for Case 2; slots 6 and 7 for Case 5; and slots 2 and 3 for Case 7), and finally, Cases 3 and 6 place the transmitter in the third slot and the receiver in the second (slot numbers 11 and 6 for Case 3; slots 7 and 6 for Case 6). Further, in Case 1, we position the antennas 180° apart in the radome (labeled in the table as ‘transmission’), and they are oriented in a co-polarized fashion. Like Case 1, Case 2 is a transmission scenario, but now the antennas are cross-polarized. Cases 3 and 4 have the antennas 90° apart in the radome, co-polarized and cross-polarized, respectively. We refer to Cases 3 and 4 as ‘scattering’ scenarios, in which the signal at the received antenna may be a combination of waves reflected off of the tumor and transmitted through it. In both cases, there are two tumor sites: in the center of the radome, and halfway between the center and the wall adjoining the two antenna positions. Finally, Cases 5-7 are the reflection scenarios. In Cases 5 and 6, the antennas are co-polarized, while in Case 7 they are cross-polarized. Cases 5 and 6 appear the same in the table, the difference between them is that the transmit and receive antenna have swapped slots (*i.e.* in Case 5 the transmitter and receiver are in slots 6 and 7, respectively; and in Case 6 they are in 7 and 6, respectively). In all three, there is a tumor site in the center of the radome and another halfway between the center and the radome wall where the antennas are located.

Table I

Description of measurement cases for Test 1. The diagrams depict the radome, antennas and breast phantom, as seen from the chest wall looking into the breast. The large blue circle represents the radome, and the beige the breast phantom. The heart-shaped antennas are parallel to our view, while a solid line means the antenna is perpendicular to this view. Hollow shapes within the breast phantom are tumor sites: a purple circle is a site centered in the radome, and a red diamond is a site halfway between the center of the radome and the radome wall.

| Case | Schematic | Polarization | Test scenario |
|------|-----------|--------------|---------------|
| 1 | | Co- | Transmission |
| 2 | | Cross- | Transmission |
| 3 | | Co- | Scattering |
| 4 | | Cross- | Scattering |
| 5 | | Co- | Reflection |
| 6 | | Co- | Reflection |
| 7 | | Cross- | Reflection |

In all cases, the tumors are placed at maximum depth (*i.e.*, near the chest wall), as a wave travelling to this position will cover more distance and thus experience higher attenuation than for other positions.

Test 2 Description: Homogeneous Breast Phantoms with Skin

Test 2 examines the performance of our system with slightly more realistic breast phantoms: the fat-only phantoms are now covered by a 2.5-mm thick layer of skin. Thus, we are still testing a homogeneous tissue case. In Test 2, the frequency of the system clock is 250MHz.

The cases we measure in Test 2 are all the same as they were in Test 1. Thus, the 39 measurements described by Table I are repeated in this test for a breast phantom that has skin. The tumor sizes, likewise, are the same as in Test 1. We presented Test 2 initially in (9); here the results are shown in a different light.

Test 3 Description: Heterogeneous Breast Phantoms with Skin

Test 3 explores the testing of our system with our most complex breast phantoms to date. We now use heterogeneous breast phantoms that have the thin skin layer filled with a combination of adipose- and glandular-mimicking tissues. This final series of tests also benefits from lessons learned in Test 1 and Test 2. For Test 3, the clock frequency is only 25 MHz. Also, as will be seen below, antenna arrangements that failed or performed poorly in Test 1 and Test 2 are not re-tested here. As well, in order to fully explore the detection capability of our system, the tumor sizes in Test 3 include much smaller tumors than were used in earlier tests.

The procedure for making phantoms with glandular structures is more complex than making homogeneous fat-only phantoms. The steps are as follows. First, we create the skin layer and allow it to harden. While it is hardening, we mix the glandular phantom and pour into moulds. We use conical shaped moulds for this work, with volumes of either 27 mL or 30 mL. The gland and skin solidify for 1-2 days before ready for use. Once hard, the glands are trimmed as necessary to satisfy volume requirements and placed randomly within the skin; the remaining space around them is filled with fat phantom. The process is described in more detail in (21). For Test 3, we experiment with different concentrations of glandular content in our heterogeneous phantoms. More specifically, we design and build phantoms that have 30%, 50%, 80% and 100% gland content (with the rest of the phantom being filled with fat, when necessary). For example, the 30% gland phantom will contain 30% glandular-mimicking tissue in the breast interior, by volume, and 70% fat-mimicking tissue; and the 100% gland phantom contains 0% fat-tissue.

Since mammography struggles most with tumor detection in denser breast tissues (3), it is vital that a supplementary breast cancer detection technique be successful in such a scenario. In fact, a study reported in (22) shows that 63% of women aged 25-29 have more than 50% glandular content in their breasts, while 24% of women aged 75-79 have more than 50% glandular content. These statistics emphasize the need for our system to be successful in detecting tumors in breast phantoms with high amounts of glandular tissue. For the 50% and 80% glandular-content phantoms, there are a high number of interfaces between various tissue types, thus significantly increasing the detection challenge over the 30% gland and the purely adipose breast phantoms. However, since breast composition varies significantly from person to person and even from breast to breast, it is impossible to quantify the physiological shape or precise dimensions of glandular structures. Therefore, we do not attempt to match our phantoms exactly to any actual given breast, but rather to provide a breast model that contains the correct tissue types in appropriate concentrations relative to common breast

Table II

Number of glandular structures in each heterogeneous phantom.

| % Glandular content | # Glandular structures |
|---------------------|---------------------------|
| 30 | 7 |
| 50 | 10 |
| 80 | 13 |
| 100 | 1 (filling skin entirely) |

densities. The complete breast phantoms seen here are among the most realistic that have been developed so far, and accordingly provide a good basis for system testing. Thus while the gland phantoms are not exact matches to their corresponding anatomical structures, we feel that the phantoms used in this way present a significant increase in the detection challenge, and are therefore a useful step forward in identifying whether or not our system can successfully operate under more complicated situations.

Table II shows the number of glandular structures incorporated into the phantoms of each glandular concentration. It gives the number of conical gland structures that it takes to fill the required volume of glandular tissue. Depending on the desired volume of glandular tissue, the conical structures we use may be full-sized or cut to a partial size. Also, we count the 100% gland phantom as having one glandular structure, even though it does not contain conical-shaped glands but rather has a homogeneous gland filling entirely the skin. As an example, Figure 5 shows a picture of the partially



Figure 5: Photograph of partially completed 30% gland phantom, with seven glandular structures.

completed 30% gland phantom, taken just before the fat was added to the phantom. In the photograph, we can see seven conical gland structures, of varying sizes, arranged randomly within the skin. Another example, pictured in Figure 6, is the partially completed 80% gland phantom containing 13 gland structures.

The antenna arrangements in Test 3 are limited to Cases 5, 6 and 7. These reflection scenarios were the ones for which the system performed best in Tests 1 & 2. Further, measuring a reflection scenario instead of a transmission scenario makes sense – the distance the wave propagates through the breast is always less for reflected waves than transmitted, except when the tumor is positioned exactly at the breast center (which is unlikely to occur in nature). Less propagation distance corresponds to less attenuation, and thus we hope to receive larger signals for the reflection scenarios than the transmission scenarios.

The tumor sites in Test 3 are also limited compared to Tests 1 and 2. As mentioned in the above paragraph, for the reflection scenario cases, a tumor should always be closer to the antennas than the center of the radome. Thus, we test only one tumor site – halfway between the radome center and the antennas. At this distance, we place three different sized tumors in turn, all spherical, with diameters of 0.5 cm (smallest size, ‘S’), 1 cm (medium, ‘M’), and 2 cm (large, ‘L’). All tumors are placed at a depth of 0.5-1 cm from the chest wall.



Figure 6: Photograph of partially completed 80% gland phantom, with 13 gland structures (nine along outer surface, an additional four inside).

Test 4 Description: Comparison of Matching Media

As a final test, we briefly examine the use of two different matching media in our system. In Tests 1, 2 and 3, all measurements were performed using the fat-mimicking material as the matching medium. However, we wish to further test whether the gland-mimicking matching medium will provide better system performance for the case of phantoms with high glandular content.

The antenna substrate and radome both have relative permittivity close to 10. Recent measurements have shown fatty tissue to have $\epsilon_r \approx 5$ at 5 GHz, and glandular tissue $\epsilon_r \approx 45$ at 5 GHz (23). Thus the fat-mimicking matching medium should provide fewer reflections in a fat-dominated breast phantom, and the gland-mimicking medium should work better for more heterogeneous phantoms. We note that this effect will be diminished by the need to use the radome, which will induce a slight mismatch with the fat-mimicking material and a larger mismatch with the gland-mimicking material as matching mediums.

We run the same measurements as in Test 3, repeated for a 100% gland phantom with a gland-matching medium. We compare these experimental results with the data presented for Test 3 with a 100% gland phantom and a fat-mimicking matching medium.

Calculating the Tumor Response

To analyze the measurement data, we calculate the tumor responses. In order to compare cases easily, we use the metric ‘T’, the tumor response relative to the input. More specifically, T is calculated, in decibels, as follows:

$$T = 20 \log_{10} \left(\frac{\max |\text{tumor response}|}{\max |\text{input pulse}|} \right) \quad [1]$$

where the maximum of the absolute value of the input pulse, measured at the antenna feed point, is the same in all cases, 6.337 V.

Further, since the value of T at which a tumor response is detectable can vary due to the different levels of background noise and clutter in each subcase, we define a second binary metric. The tumor is considered ‘detected’ if the tumor response shows a periodic, time-domain signal that is clearly and easily seen above the background signal level. If the tumor response cannot be distinguished as being either periodic (with frequency of 250 MHz [or 25 MHz in later measurements], as this is the input pulse repetition rate), or is not visibly above the noise level, then the tumor is considered ‘undetected’.

Results and Discussion

Test 1 Results: Fat-Only Breast Phantoms

Table III provides a summary of results for Test 1. For each case, the table lists the average, best and worst relative tumor responses. These values are obtained by examining each subcase: for instance for Case 3, we find the average, maximum and minimum relative tumor responses over the set of four relative tumor responses (2 cm tumor in center, 1 cm tumor in center, 2 cm tumor halfway between center and radome wall, and 1 cm tumor halfway between center and radome wall). For all subcases of Test 1, the tumor responses fall into the 'detected' category.

As an example, we also plot a sample tumor response in Figure 7. This time-domain signal corresponds to two periods of the tumor response for Case 6, with the 1 cm tumor in the site halfway between the center of the radome and the antennas. This particular subcase is the one in which the peak relative tumor response was the best, out of all the other subcases in Test 1, with a value of -40.3 dB.

To summarize, in Test 1, examining a homogeneous phantom made entirely of adipose tissue, we see that all seven antenna arrangements easily detect both the 2 cm and 1 cm tumors, at all tested positions. We note from Table III that for the reflection scenarios Cases 5 and 6, the system performs better on average than for the transmission scenarios Cases 1 and 2, and in fact all other cases. Further, Case 2 has the lowest average relative tumor response out of all the cases

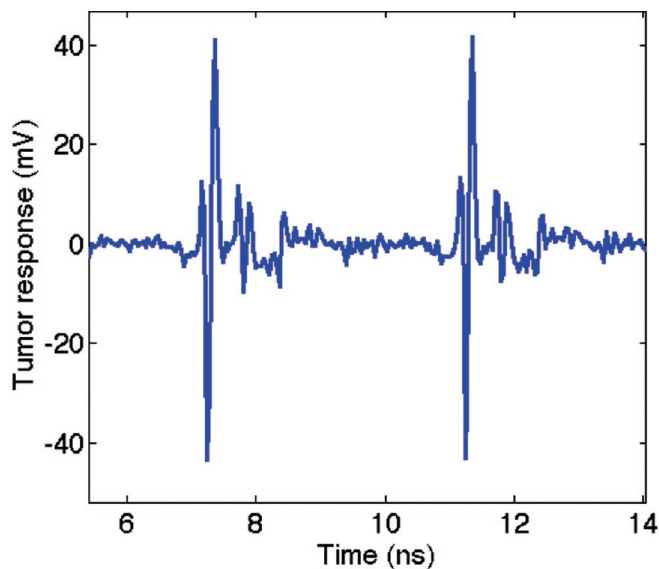


Figure 7: Two periods of the tumor response for Case 6, with a 1-cm tumor placed at the site halfway between the radome center and the antennas. This subcase corresponds to the best T obtained in Test 1.

Table III

Summary of Test 1 measurements.

| Case # | Average T (dB) | Worst T (dB) | Best T (dB) |
|--------|----------------|--------------|-------------|
| 1 | -55.8 | -66.2 | -49.2 |
| 2 | -67.0 | -69.8 | -65.2 |
| 3 | -53.8 | -64.2 | -48.0 |
| 4 | -55.4 | -70.6 | -46.9 |
| 5 | -43.2 | -45.7 | -41.9 |
| 6 | -41.2 | -42.4 | -40.3 |
| 7 | -57.3 | -60.1 | -53.3 |

with -67.0 dB, and Case 6 has the highest with -41.2 dB, making a difference of almost 26 dB between the best and worst cases. Even the worst tumor responses for Cases 5 and 6 are better than the best responses for all other cases. This suggests that our system provides the best tumor detection performance using Cases 5 and 6 on this fat-only phantom.

Test 2 Results: Homogeneous Breast Phantoms with Skin

We present the measurement results for Cases 1 to 7 for our breast phantom with skin in Table IV. As in Table III, the average, best and worst T values are provided for each case. Further, Figure 8 plots a sample tumor response, here for Case 7 with a 1-cm diameter tumor placed halfway between the radome center and the antennas. This particular subcase is the scenario for which our system performs best, as per Table IV.

In Test 2, as in Test 1, both tumors are detected in every position with every antenna arrangement. In some subcases, for instance, Case 1 with a tumor in the radome center (both sizes of tumors), the tumor response is approaching the lower detection limit. However, at this stage of phantom complexity, the tumor is successfully detected in all subcases. The results of Test 2 indicate that the addition of a skin layer does not prevent detection for a homogeneous phantom.

From Table IV, we note that with the Case 7 antenna arrangement our system performed better than all other cases, with an average relative tumor response of -50.9 dB, and a best-case

Table IV

Summary of Test 2 measurements.

| Case # | Average T (dB) | Worst T (dB) | Best T (dB) |
|--------|----------------|--------------|-------------|
| 1 | -63.6 | -68.9 | -59.6 |
| 2 | -65.6 | -71.5 | -62.5 |
| 3 | -65.0 | -71.8 | -60.1 |
| 4 | -55.0 | -56.1 | -53.4 |
| 5 | -54.4 | -58.0 | -51.6 |
| 6 | -62.7 | -69.8 | -53.9 |
| 7 | -50.9 | -56.3 | -47.3 |

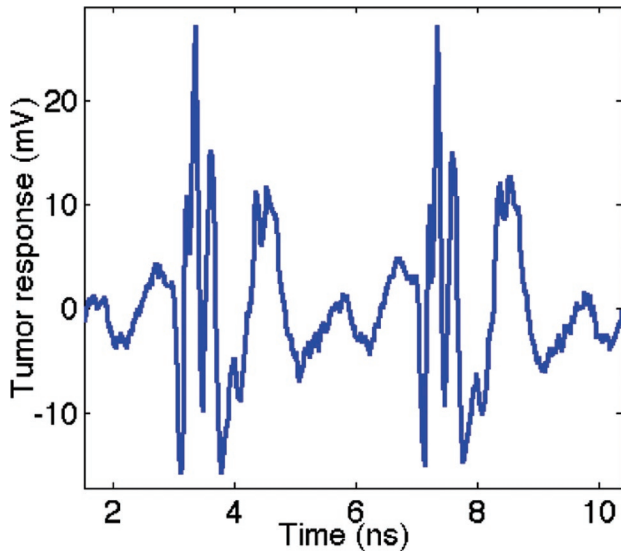


Figure 8: Two periods of the tumor response for Case 7, with a 1-cm tumor placed at the site halfway between the radome center and the antennas. This subcase corresponds to the best T obtained in Test 2.

relative tumor response of -47.3 dB. The second best detection scenario was found to be Case 5, with an average T of -54.4 dB and a best of -51.6 dB. It is interesting that both of the two best cases are reflection scenarios, as were the two best cases of Test 1. However, unlike Test 1, the best case in Test 2 is one with a cross-polarized antenna arrangement. In fact, comparing the average T in the first columns of Tables III and IV, for fat-only and fat with skin phantoms, respectively, we see that the system detecting with perpendicularly-oriented cases (2, 4 and 7) for the phantoms with skin outperform these same cases for the phantoms without skin. On the other hand, the cases with co-polarized antennas (1, 3, 5 and 6) have higher average T's for the fat-only phantoms than for the phantoms with skin. This confirms the trend discovered in (20), and suggests that the skin plays a significant role in the polarization of the received signal, indicating that both co-polarized and cross-polarized tumor responses may be useful for detection purposes. This realization also shows that the skin layer does not necessarily hinder the tumor detection ability of a system, as long as the antenna arrangements are carefully chosen.

We also see from the results in Table IV that for Test 2 it is Case 2 in which our detection system performs the most poorly. In Test 1, it was also Case 2 that had the worst results, so it is likely Case 2 is not a useful choice of antenna arrangements for tumor detection.

From the plots in Figures 7 and 8, we note that the best-case tumor response with skin still has a lower amplitude than the best-case response without skin, as could be predicted since the skin layer adds reflections and attenuation to the signal. More importantly, in Figure 8 the two successive periods of the tumor response are not distinct – they overlap. This indicates that a new pulse is being transmitted into the system before the first one has had sufficient time to die out; an effect that was not seen in Test 1 when there was fewer tissue interfaces present. Because of this observation, we decrease the input signal's repetition rate by a factor of 10 to 25 MHz in all later measurements. This decrease is beneficial in two ways: not only do signals no longer overlap, leading to cleaner results, but there is also less energy transmitted into the breast in a given scan time. Also, decreasing the clock frequency does not necessarily increase the amount of time required for a scan, as only one period of the received signal is really needed for an analysis (since each period reproduces the signal identically).

Test 3 Results: Heterogeneous Breast Phantoms with Skin

We present the measurement results for the 30%, 50%, 80% and 100% glandular content breast phantoms for Cases 5, 6 and 7 in Table V. The table shows the T-value (peak tumor response, in dB) for the small, medium and large tumor sizes that we tested. It also provides an average T for each glandular phantom – a value that gives an indication of the difficulty of detecting a tumor in a breast phantom with the given amount of glands. Further, the shaded cells in Table V illustrate the situations in which detection of the tumor failed. In other words, for the shaded cell subcases, T is at such a level that it is below the background noise, or clutter.

In Figure 9, we plot a selected example of the time-domain tumor response: a 50% gland phantom tested with the Case 5 antenna arrangement and a medium-sized tumor. This

Table V

Summary of Test 3 measurements. For each phantom with different percentages of glandular content, the peak tumor response in dB is given for the small ('S'), medium ('M') and large ('L') tumor in Cases 5, 6 and 7. A shaded cell indicates this tumor response is not detectable. The average peak tumor response for each phantom is also provided.

| | Case 5 (dB) | | | Case 6 (dB) | | | Case 7 (dB) | | | Average (dB) |
|------------|-------------|-------|-------|-------------|-------|-------|-------------|-------|-------|--------------|
| | S | M | L | S | M | L | S | M | L | |
| 30% Gland | -56.9 | -54.4 | -51.5 | -51.4 | -51.9 | -52.6 | -63.8 | -65.9 | -53.1 | -55.7 |
| 50% Gland | -55.2 | -49.8 | -49.2 | -55.3 | -52.4 | -52.1 | -65.4 | -64.4 | -65.4 | -56.6 |
| 80% Gland | -48.5 | -45.2 | -38.7 | -52.2 | -47.0 | -46.1 | -47.9 | -48.9 | -48.0 | -46.9 |
| 100% Gland | -64.4 | -60.3 | -57.8 | -62.8 | -60.5 | -58.4 | -63.4 | -64.7 | -64.2 | -61.8 |

scenario is one in which the tumor was successfully detected – as can be seen from the tumor response, which is clean and several millivolts above the noise level. Also in Figure 9, we provide an example of a tumor response for which the tumor was considered undetectable. This tumor response is for the 30% gland phantom, for a small tumor with antennas arranged as per Case 7. In this subcase, the peak tumor response is at the same level as the background noise, so even though we see a hint of the tumor response’s shape within the noise, detection is considered to have failed.

The results we have presented for Test 3 up to this point, and for Test 1 and 2 as well, have all been considered in the time-domain. Now, for Test 3 alone, we will delve into a brief analysis of the results in the frequency domain. We present this aspect for Test 3 only because heterogeneous breast phantoms are the most realistic and present the greatest challenge to successful tumor detection. Thus, we carefully examine the measurement results for the glandular phantoms with the goal of identifying any room for improvement in our detection system.

We analyze the frequency content of the tumor responses for the 30%, 50% and 80% gland phantoms. If the system could operate using the ultrawideband (UWB) range (3.1 – 10.6GHz), it would allow use of already existing technologies: pulse generators, antennas, *etc.* With this in mind, we calculate the percentage of signal content of each tumor response that is within the 3 to 10GHz range. The

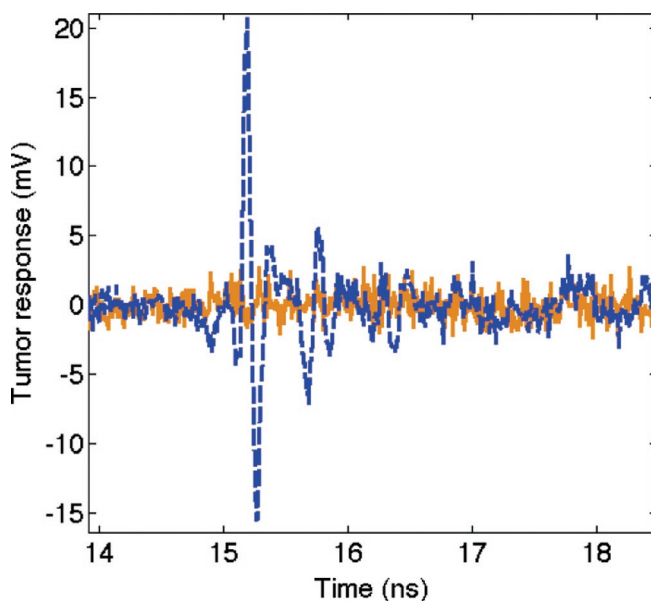


Figure 9: Tumor response for 50% gland phantom, Case 5, medium tumor (blue, dashed), in this scenario, our system easily detects the tumor; and tumor response for 30% gland phantom, for a small tumor with antennas arranged as per Case 7 (orange, solid), a failed detection scenario.

pulse we input into our system from the impulse generator has a very short duration, however it does not cover solely the UWB range; in actuality, 57.8% of its power is outside the desired frequency band. This is the reason our calculated tumor responses have content outside of the UWB range. Table VI presents the average (over the small, medium and large tumors) percentage of the tumor response content that is within the 3 to 10GHz range, for each case of each gland phantom.

To give a better idea of the frequency spectrum seen in tumor responses, we show examples from a high glandular content breast phantom. Figure 10 plots the normalized frequency content of the tumor response up to 10GHz for the 80% gland phantom, measured with Case 7 and all three sizes of tumors. Figure 11, similarly, plots the frequency spectrum of the same phantom for Case 5.

This section has presented the results of our system’s tumor detection on heterogeneous phantoms made up of 30%, 50%, and 80% glandular content; as well as a homogeneous 100% gland breast phantom. From Table V, we note most importantly that for every breast phantom, each tumor is detected by at least one antenna arrangement. Overall, our system successfully detected the tumor in 32 out of 36 subcases.

Examining Table V, and comparing to the results in Tests 1 and 2, we see that the detectable level for a tumor response is decreased for heterogeneous phantoms, and the 100% gland phantom, as compared to the homogenous fat-filled phantoms. For instance, in Table III (Test 1 results), we see the smallest tumor response was at -70.6 dB; and in Table IV (Test 2 results) the smallest is -71.8 dB. Both of these tumors were detected by the system. However, from Table V, the Test 3 results show that tumor responses at -63.8 dB, -64.4 dB and -65.4 dB fail to be detected. This suggests that, due to the high attenuation of the glandular-mimicking tissue, and the structures internal to the breast phantom, the background noise of the system is increased for phantoms with glands. The increase in background clutter arises with a number of internal reflections occurring from the transmitted pulse bouncing off of the gland structures; signal content that is not useful to us.

Table VI

Average percentage of tumor response in the 3-10GHz range for the 30%, 50% and 80% glandular content breast phantoms as recorded from Cases 5, 6 and 7.

| | Case 5 | Case 6 | Case 7 |
|-----------|--------|--------|--------|
| 30% Gland | 67.0% | 73.1% | 66.5% |
| 50% Gland | 54.4% | 63.8% | 71.7% |
| 80% Gland | 59.5% | 43.2% | 31.2% |

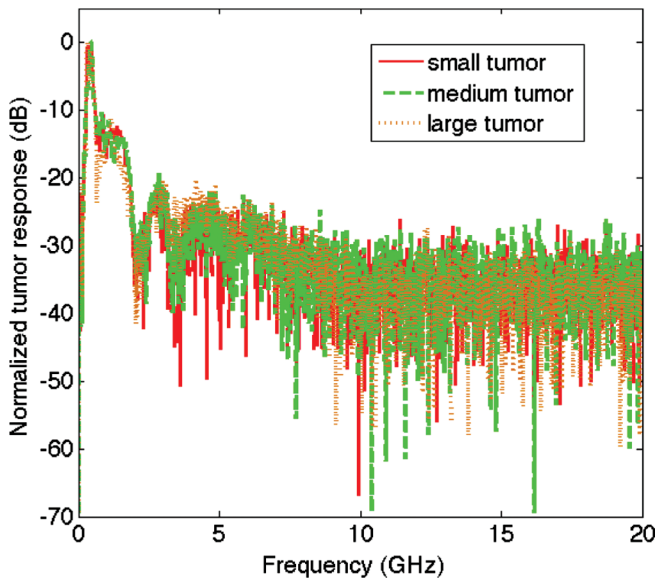


Figure 10: Normalized tumor response in the frequency domain for the 80% gland phantom, Case 7, with small tumor (red, solid line); medium tumor (green, dashed line); and large tumor (orange, dotted line).

We also see that tumor responses at a certain level can be detected in some situations, but not in others. For example, in the 30% gland phantom, Case 7 with a small tumor, the tumor response is at -63.8 dB. In this particular scenario, this tumor response is undetectable by our system. Yet, in the 50% gland phantom, Case 7 with a medium tumor, the peak tumor response is even lower, at -64.4 dB, and is detectable. Thus there is no absolute cut-off level below which

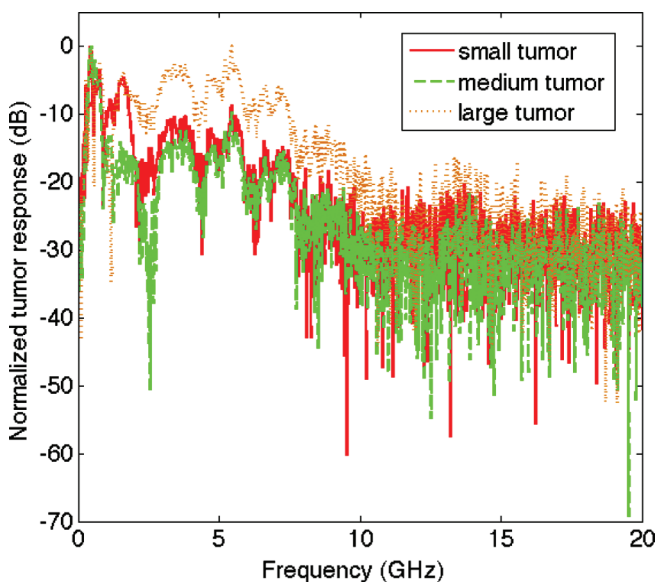


Figure 11: Normalized tumor response in the frequency domain for the 80% gland phantom, Case 5, with small tumor (red, solid line); medium tumor (green, dashed line); and large tumor (orange, dotted line).

the tumor response is undetectable – whether a given level of tumor response can be detected or not depends on the breast phantom’s contents, physiological layout, and antenna arrangement.

Another interesting point that we observe from Table V is that the tumor response (and detection ability of our system) does not necessarily improve with decreasing percentage of gland in the phantom. Due to the various arrangements of the individual glandular structures within the breast phantom, glands could likely affect the tumor response more significantly in some arrangements than others. That is, if the gland happens to be located directly in front of the transmitting antenna, and a tumor is on the other side of the gland, our system may experience difficulties detecting the tumor. However, if the antennas happened to be placed in between two adjacent glandular structures, detection may be easier. Thus it is important not to assume that a higher fat content in the test phantom automatically implies an easier system test scenario.

Finally, we note that there is no single antenna arrangement that gives the best system performance for all subcases (seen in Table V). For the 30% gland phantom with a large tumor, Case 5 provides the best tumor response. For the 100% gland phantom with a small tumor, the tumor response from Case 6 is the best; while for the 80% gland phantom with a small tumor it is Case 7. This confirms that an antenna array for use with our system should include all three antenna arrangements (Cases 5, 6 and 7) in order to maximize system performance.

The frequency content of the tumor responses provide a measure of our system’s efficiency in the UWB frequency range. From Table VI and Figure 10, it is clear that for the 80% gland phantom, Case 7 is an antenna arrangement that leads to very little tumor response content in the UWB range. In fact, only 31.2% of the tumor response, on average, is in the desired band. Also, very little of the signal content, if any, is useful above 5 GHz. On the other hand, the same gland phantom tested using Case 5 has a tumor response that covers the UWB range better. From Table VI and Figure 11, we see that this antenna arrangement results in a tumor response that has almost 60% of its power in the UWB range, double the value for Case 7. Further, from Figures 10 and 11, we observe that there is no useful content above 8 GHz in either case scenario. Thus, this data suggests that if UWB operation is indeed desired, then our system could be much more efficient using the Case 5 antenna layout with a specially designed pulse, one that does not have significant power below 3 GHz nor above 8 GHz. In this way, the power will be focused in the UWB range and will likely provide better tumor responses. However, since significant tumor responses are seen below 3 GHz, the UWB

range maybe not be the most optimal choice for successful tumor detection.

Test 4 Results: Comparison of Matching Media

Table VII lists the peak received signals for the gland- and fat-matching media, for Cases 5, 6 and 7 with the three sizes of tumor. Similarly, Table VIII gives the peak tumor responses for the same set of measurements. In Table VIII, the shaded cells imply a subcase for which the tumor response was undetectable (as in Table V).

From Table VII, we see that in Cases 5 and 6 the gland-matching medium leads to improved received signals over the fat-matching medium, however, in Case 7 the opposite occurs. Despite this, the maximum difference in the peak received signal between the gland-matching medium and the fat-matching medium for all subcases does not exceed 3.6 dB. In Table VIII, we see immediately that the small tumor with antennas in arrangement Case 5 is not detectable by our system with either matching medium. For six of the remaining eight subcases, the peak tumor response is improved by an average of 1.77 dB by using the gland-matching medium. For the remaining two subcases the fat medium provides an average improvement of 0.7 dB with respect to the usage of the gland material.

Overall, even with high glandular content in breast phantoms, the gland-matching medium does not provide significant advantage over the fat-mimicking material. This supports our decision to report our experimental results obtained with the fat-matching medium. Nonetheless, as a possible point for future work, we note that the choice of the matching medium does influence the system's detection performance. As the patient breast content is often unknown, an optimized procedure could include measurements with several matching media.

Table VII

Peak received signals (in dB, relative to the peak input voltage) for Cases 5, 6 and 7, with small ('S'), medium ('M') and large ('L') tumors, measured with fat- and gland-matching media (MM).

| | | Fat-MM (dB) | Gland-MM (dB) |
|--------|---|-------------|---------------|
| Case 5 | S | -43.2 | -40.5 |
| | M | -43.0 | -40.4 |
| | L | -43.0 | -40.4 |
| Case 6 | S | -42.7 | -39.2 |
| | M | -42.7 | -39.1 |
| | L | -42.5 | -38.9 |
| Case 7 | S | -48.5 | -48.9 |
| | M | -48.5 | -48.6 |
| | L | -48.5 | -48.9 |

Table VIII

Peak tumor responses (in dB, relative to the peak input voltage) for Cases 5, 6 and 7, with small ('S'), medium ('M') and large ('L') tumors, measured with fat- and gland-matching media (MM).

| | | Fat-MM (dB) | Gland-MM (dB) |
|--------|---|-------------|---------------|
| Case 5 | S | -64.4 | -64.9 |
| | M | -60.3 | -58.3 |
| | L | -57.8 | -58.4 |
| Case 6 | S | -62.8 | -60.2 |
| | M | -60.5 | -58.8 |
| | L | -58.4 | -56.0 |
| Case 7 | S | -63.4 | -64.2 |
| | M | -64.7 | -63.8 |
| | L | -64.2 | -63.2 |

Conclusion

In this work, we have presented our initial time-domain microwave breast cancer detection system and tested its performance thoroughly with breast phantoms. We show successful detection of tumors in homogeneous fat-only phantoms, both with and without a layer of skin, as well as in heterogeneous phantoms with skin. System tests with heterogeneous phantoms of 30%, 50% and 80% glandular content demonstrate that we are able to detect tumors as small as 5 mm. Results show that operating our system with antennas positioned on the same side of the breast, in either co- or cross-polarized fashion, is the most useful for tumor detection. Future work to improve the ease of tumor detection includes implementing the optimized array, using amplifiers to slightly increase the power transmitted into the breast (within safety limits), and using a pulse more adapted to the ultrawideband frequency range.

Conflict of Interest

We certify that regarding this paper, no actual or potential conflicts of interests exist; the work is original, has not been accepted for publication nor is concurrently under consideration elsewhere, and will not be published elsewhere without the permission of the Editor and that all the authors have contributed directly to the planning, execution or analysis of the work reported or to the writing of the paper.

Acknowledgements

The authors are grateful for the funding support from the Natural Sciences and Engineering Research Council of Canada (NSERC), le Fonds québécois de la recherche sur la nature et les technologies (FQRNT), and le Partenariat de Recherche Orientée en Microélectronique, Photonique et Télécommunications (PROMPT). The authors also thank Jules Gauthier of Polytechnique Montreal for fabricating

our antennas, and Donald Pavlasek of McGill University for machining the mould used in creating the skin phantom. We also acknowledge Alexandre Bourdon and Dady Coulibaly, McGill undergraduate students, for designing and building the glandular tissue phantoms.

References

1. Lazebnik, M., Popovic, D., McCartney, L., Watkins, C., Lindstrom, M., Harter, J., Sewall, S., Ogilvie, T., Magliocco, A., Breslin, T., Temple, W., Mew, D., Booske, J., Okoniewski, M., Hagness, S. A large-scale study of the ultrawideband microwave dielectric properties of normal, benign and malignant breast tissues obtained from cancer surgeries. *Phys Med Biol* 52, 6093-6115 (2007). DOI: 10.1088/0031-9155/52/20/002
2. American Cancer Society. *Cancer Facts & Figures* (2008).
3. Fear, E., Meaney, P. M., Stuchly, M. A. Microwaves for breast cancer detection? *IEEE Potentials* 22(1), 12-18 (2003). DOI: 10.1109/MP.2003.1180933
4. Fear, E. Microwave imaging of the breast. *Technol Cancer Res Treat* 4(1), 69-82 (2005).
5. Klemm, M., Gibbins, D., Leendertz, J., Horseman, T., Preece, A., Benjamin, R., Craddock, I. Development and testing of a 60-element UWB conformal array for breast cancer imaging. *Antennas and Propagation (EUCAP), Proceedings of the 5th European Conference on*, 3077-3079 (2011).
6. Golnabi, A., Meaney, P. M., Geimer, S., Paulsen, K. D. Microwave imaging for breast cancer detection and therapy monitoring. *Biomedical Wireless Technologies, Networks, and Sensing Systems (BioWireless), 2011 IEEE Topical Conference on*, 59-62 (2011). DOI: 10.1109/BIOWIRELESS.2011.5724347
7. Meaney, P. M., Fanning, M., Reynolds, T., Fox, C., Fang, Q., Kogel, C., Poplack, S., Paulsen, K. Initial clinical experience with microwave breast imaging in women with normal mammography. *Acad Radiol* 14(2), 207-218 (2007). DOI: 10.1016/j.acra.2006.10.016
8. Byrne, D., O'Halloran, M., Glavin, M., Jones, E. Breast cancer detection based on differential ultrawideband microwave radar. *Prog Electromagn Res* 20, 231-242 (2011). DOI: 10.2528/PIERM11080810
9. Porter, E., Santorelli, A., Coates, M., Popović, M. An experimental system for time-domain microwave breast imaging. *Antennas and Propagation (EUCAP), Proceedings of the 5th European Conference on*, 2906-2910 (2011).
10. Picosecond Pulse Labs. [Online]. Available: <http://www.picosecond.com/> (2011).
11. Tektronix. [Online]. Available: <http://www.tek.com/> (2011).
12. Pico Technology Limited. [Online]. Available: <http://www.picotech.com/> (2011).
13. Kanj, H., Popović, M. A novel ultra-compact broadband antenna for microwave breast tumor detection. *Prog Electromagn Res* 86, 169-198 (2008). DOI: 10.2528/PIER08090701
14. Friatec. [Online]. Available: <http://www.friatec.com/> (2011).
15. Emerson & Cuming Microwave Products. [Online]. Available: <http://www.eccosorb.com/> (2011).
16. Porter, E. Microwave breast tumor detection: simulation and design of experiments with tissue phantoms. *Master's Thesis, Department of Electrical and Computer Engineering, McGill University, Montreal, Canada* (2010).
17. Porter, E., Fakhoury, J., Oprisor, R., Coates, M., Popović, M. Improved tissue phantoms for experimental validation of microwave breast cancer detection. *Antennas and Propagation (EUCAP), Proceedings of the 4th European Conference on*, 1-5 (2010).
18. Santorelli, A. Breast screening with custom-shaped pulsed microwaves. *Master's Thesis, Department of Electrical and Computer Engineering, McGill University, Montreal, Canada* (2012).
19. Klemm, M., Leendertz, J., Gibbins, D., Craddock, I., Preece, A., Benjamin, R. Microwave radar-based breast cancer detection: imaging in inhomogeneous breast phantoms. *IEEE Antennas Wireless Propag Lett* 8, 1349-1352 (2009). DOI: 10.1109/LAWP.2009.2036748
20. Porter, E., Santorelli, A., Coates, M., Popović, M. Microwave breast imaging: time-domain experiments on tissue phantoms. *Antennas and Propagation (APSURSI), 2011 IEEE International Symposium on*, 695-698 (2011). DOI: 10.1109/APS.2011.5996807
21. Porter, E., Santorelli, A., Bourdon, A., Coulibaly, D., Coates, M., Popović, M. Time-domain microwave breast cancer detection: experiments with comprehensive glandular phantoms. *Microwave Conference Proceedings (APMC), 2011 Asia-Pacific*, (2011).
22. Stomper, P., D'Souza, D., DiNitto, P., Arredondo, M. Analysis of parenchymal density on mammograms in 1353 women 25-79 years old. *Am J Roentgenol* (167), 1261-1265 (1996).
23. Zastrow, E., Davis, S., Lazebnik, M., Kelcz, F., Hagness, S. Development of anatomically realistic numerical breast phantoms with accurate dielectric properties for modeling microwave interactions with the human breast. *IEEE Trans Biomed Eng* 55(12), 2792-2800 (2008). DOI: 10.1109/TBME.2008.2002130

Received: April 13, 2012; Revised: June 29, 2012;

Accepted: July 31, 2012

